Journal of Marine Research, 69, 221–244, 2011

Impacts on the global ocean circulation from vertical mixing and a collapsing ice sheet

by J. A. M. Green[1] and G. R. Bigg[2,3]

ABSTRACT

The current view of the global meridional overturning circulation (MOC) is one where the Atlantic is a dominant basin for deep water formation, but with the potential for bipolar seesaws between the Southern Ocean and the North Atlantic during catastrophic freshening events in either hemisphere. Here we investigate the stability of this paradigm through the response of an intermediate complexity coupled climate model, set in an oceanically more sensitive glacial configuration, to variation in the vertical mixing rates. It is found that the convective basin is set by the upper ocean diffusivity, with higher such diffusivities leading to a Pacific-dominated MOC. The upper ocean diffusivity is found to have a larger impact on the MOC than catastrophic flood events. It is known that deep ocean mixing rates were enhanced during glacial periods due to greater deep ocean tidal dissipation in the shallower oceans, with less extensive continental shelves. It is hypothesized that, combined with modified atmospheric states, there has been potential for the MOC to significantly alter between different glacial periods.

1. Introduction

One of the key controllers of the global climate is the oceanic Meridional Overturning Circulation (MOC). It is sustained by an input of mechanical energy from tides and winds, which induces slow large-scale vertical transports of heat and mass to balance the formation of deep-water at high latitudes (see Wunsch and Ferrari, 2004, for a review). However, large-magnitude freshwater fluxes from melting ice sheets may hamper the formation of deep water and thus act to reduce, or even shut down, the MOC in the Atlantic (e.g., Broecker and Denton, 1990; Lenderink and Haarsma, 1994; Rahmstorf, 2002; Levine and Bigg, 2008; Green *et al.*, 2009). There are several possible states of the global MOC (e.g., Kahana *et al.*, 2004), of which three relate to the Atlantic MOC: the present state with convection and deep water formation in the North Atlantic, a switched off state with only convection in the Southern Ocean, and finally a reversed state with the deep water formation in the Northern Hemisphere taking place in the North Pacific. Because of the sensitivity of the

1. School of Ocean Sciences, College of Natural Sciences, Bangor University, Menai Bridge, LL59 5AB, United Kingdom.
2. Department of Geography, University of Sheffield, Sheffield, S10 2TN, United Kingdom.
3. Corresponding author. ***email: grant.bigg@sheffield.ac.uk***

MOC to large-scale buoyancy fluxes, a sudden major input of freshwater from the collapse of a large ice sheet, e.g., the Laurentide at the termination of the last glaciation, may have had a significant effect on the oceanic and atmospheric circulation, hydrological balance, biology and sedimentation in the Atlantic Ocean. At the same time the ocean during the last glaciation was more energetic due to enhanced tides (e.g., Egbert *et al.*, 2004; Green, 2010), which may have led to an enhanced vertical diffusivity in the abyssal ocean. The present paper therefore investigates the sensitivity of, and effects on, the large-scale overturning circulation of freshwater pulses from a collapsing Laurentide Ice Sheet at the end of the last glaciation in combination with altered vertical global mixing rates. More specifically, we investigate if altered vertical mixing rates in the upper and/or abyssal ocean can change the state of the MOC from being dominated by the Atlantic, as it is at present and potentially was during the last glacial maximum (LGM), to the Pacific or Southern Ocean.

The majority of the marine-terminating areas of glacial ice sheets probably melted over a relatively short time-span of about 500 years, and their oceanic discharge may therefore be described as a 'collapse' or very rapid deglaciation (e.g. Bischof, 2000). The Barents Ice Sheet most likely seeded large icebergs and ice streams at the end of the glacial, whereas the Laurentide, which is under investigation here, rapidly discharged freshwater from ice lakes straight into the northern polar seas, triggering the Younger Dryas event some 12,500 years BP (Bradley *et al*., 1999; Teller *et al.*, 2005; Murton *et al.*, 2010). Such a sudden influx of large volumes of freshwater had a significant effect on the oceanic circulation, not only in the Atlantic but also on a global scale (MacAyeal, 1993; Alley, 1998), because of the negative feedback on the formation of North Atlantic Deep Water (NADW) and resulting reduction of the Atlantic MOC (henceforth AMOC, e.g. Keigwin *et al.*, 1991; Rahmstorf, 2002; Zhang and Delworth, 2005; Stouffer *et al.*, 2006). This had an impact on ocean temperature and thus heat transport and in the end, led to a temporarily cooler climate (Keigwin *et al.*, 1991; Vellinga and Wood, 2002; Schmittner *et al.*, 2003).

During the LGM the present shelf seas were largely absent due to a 120–140 m drop in sea-level (Fairbanks, 1989; Yokoyama *et al.*, 2000). This caused a 20% increase in the global tidal dissipation, and more than 50% of the total tidal energy dissipated in the deep ocean compared to about 30% at present (Egbert *et al.*, 2004; Green, 2010). The rapid deglaciation of the Barents and the Laurentide Ice Sheets is thus associated with a very rapid sea-level rise that flooded vast areas currently forming shallow shelf seas and significantly modified the tidal dissipation regime. At the same time, there is strong evidence from both paleoclimatic data records and model simulations that the (Atlantic) MOC has changed magnitude in the past (Bigg *et al.*, 2000; Duplessey, 2004), including complete shutdowns or reversals (e.g., Seidov and Maslin, 1999; Swingedouw *et al.,* 2009; Bigg *et al.,* 2011). Some coupled model experiments of freshwater perturbations exhibit a continued MOC shutdown or reduction after the perturbation is removed (Schmittner *et al.*, 2003; Green *et al.*, 2010), while others show a recovery of the MOC within a few centuries (Vellinga and Wood, 2002; Green *et al.*, 2009). The sensitivity of the MOC to freshwater pulses, and its ability to recover, have been put down to several complex mechanisms, including enhanced paleomixing (Green *et al.*,

2009), the structure of the vertical mixing in the models (Samelson, 1998; Marzeion and Levermann, 2009), the opening of the Bering Strait, and atmospheric pathways between the Atlantic and the Pacific (Okumura *et al.*, 2009).

The rate of vertical mixing in the ocean, and the way it is implemented in ocean models, is through the vertical diffusivity, k_z, which depends directly on the rate of dissipation of mechanical energy and inversely on the buoyancy frequency (See, e.g., Osborn, 1980, for a discussion). Theoretically, an increased dissipation leads to a stronger vertical mixing (assuming the stratification evolves slowly), and we would thus see a stronger MOC (e.g. Huang, 1999). However, modeling suggests that the interaction between freshwater pulses, mixing, and the MOC led to a reduced MOC during the LGM, yet one that recovered fully after freshwater pulses because of the enhanced mixing rates (e.g., Green *et al.*, 2009). Thus, there is conflicting evidence available on the impact of freshwater pulses and vertical mixing on the state of the MOC, and there is support for the collapse of the AMOC during the Younger Dryas, associated with an ice-dam collapse from the melting Laurentide Ice Sheet (e.g., Murton *et al.*, 2010). At the same time, the flooding of the shelf seas transferred mechanical energy from the deep ocean to shallower waters which may further have reduced the strength of the AMOC. The effects on the AMOC of a combination of enhanced diffusivity and freshwater from the Barents Ice sheet collapse was investigated in Green *et al.* (2009). Here we build on their conclusions to investigate the effect on the ocean by the collapse of the Laurentide Ice Sheet in conjunction with modified magnitude and vertical structure of the diffusivity. The response of the ocean to these changes is described in terms of the strength of the Atlantic and Pacific MOCs, the location of deep water formation and convection, and calculations of the freshwater height in the upper part of the water column and the implicit ocean dissipation rates. Our answer lies in simulations using Frugal (the Fine ResolUtion Greenland And Labrador Sea model) – an intermediate complexity coupled atmosphere-ocean-sea ice-iceberg model set up for both the present and the paleo-ocean. Frugal is described in the next section together with the modifications made in terms of freshwater pulses and vertical diffusivity amendments. Section 2 also contains a summary of the simulations performed, and the results from these are presented in Section 3. A discussion and conclusions close the paper in Section 4.

2. Frugal

a. Model summary

Frugal is a global intermediate complexity coupled atmosphere-ocean model (Bigg and Wadley, 2001; Levine and Bigg, 2008), which has been used extensively to investigate the ocean and climate from the LGM to the present and is thus a reliable and well motivated choice of model. Bigg *et al.* (2000) used it to simulate and describe the Last Glacial Maximum ocean circulation, and Bigg *et al.* (1998) looked into two ocean states of the MOC during the LGM. Bigg and Wadley (2001) showed that the strength of the MOC is sensitive to the magnitude of ice albedo. Wadley and Bigg (2002) concluded that the flow through the

Canadian Archipelago and Bering Strait affects the North Atlantic circulation and that these seaways should be represented in ocean general-circulation studies. Wadley *et al.* (2002) modeled oceanic $\delta^{18}O$ distributions during the PD and LGM. More recently, Green *et al.* (2009) looked at the impact of freshwater supply from the Barents Ice Sheet and overall vertical diffusivity on the strength of the AMOC. Levine and Bigg (2008) investigated the impact of adding meltwater at iceberg source locations, and Bigg *et al.* (2011) compared the impact of different release locations on the AMOC. Here, we again look at the effect of freshwater releases but in combination with modified vertical diffusivities, concentrating on changes in either the magnitude or the vertical gradient of the vertical diffusivity.

The ocean model in Frugal has a free surface and 19 vertical layers, varying in thickness from 30 m near the surface to 500 m at depth. The model uses an orthogonal curvilinear coordinate system with the grid North Pole located in Greenland (72.5°N, 40°W) to avoid singularity points in the computational domain. This also enhances model resolution over the North Atlantic and Arctic compared to the rest of the globe. The resultant horizontal resolution is $6° \times 4°$ in the Southern Hemisphere and $1° \times 1°$ in the Nordic Seas. While this variable spatial resolution means that convective processes will be much better captured in the Northern Hemisphere, past simulations for the Present Day (PD) (e.g. Wadley and Bigg, 2002) and the LGM (e.g. Levine and Bigg, 2008) have shown realistic convective responses to model perturbations.

The bathymetry is created from ICE-5G (VM2) presented by Peltier (2004). Frugal uses the variable time-stepping method described by Wadley and Bigg (1999), where increasing numbers of shorter time steps are taken in regions of higher resolution across the model domain, whilst maintaining a synchronous integration and achieving numerical stability throughout the model. The vertical diffusivity scheme uses a horizontally constant vertical background diffusivity, k_z, which varies from $0.3\,cm^2\,s^{-1}$ in the upper 2000 m to $1.3\,cm^2\,s^{-1}$ below 3000 m depth according to (Fig. 1; Bryan and Lewis, 1979 – the present equation has been modified)

$$k_z(z) = \beta k_0 + \alpha k_r \tan^{-1}[L(100z - z_0)] \tag{1}$$

where $k_0 = 0.8\,cm^2\,s^{-1}$ is a background diffusivity, $k_r = 1.05/\pi\ cm^2\,s^{-1}$ is the vertical gradient of the diffusivity, $L = 4.5 \times 10^{-5}\,cm^{-1}$ is a length scale, z is the vertical coordinate (in meters), and $z_0 = 250000$ cm is a reference depth (note the units used). α and β are constants which are later used to obtain different mixing scenarios (see the following section). Added to k_z in the model formulation is a spatially varying isopycnal diffusivity, k_h, which mixes tracers but not momentum and which is updated following the horizontal gradients of the isotherms (Griffies *et al.*, 1998).

The atmospheric part of the model is a vertically integrated energy and moisture balance model (Fanning and Weaver, 1996) which has been modified to include advection and diffusion of heat and water vapor. The model includes parameterization of clouds, mountains, land-ice and land hydrology, and the coupling provides a grid point to grid point interactive

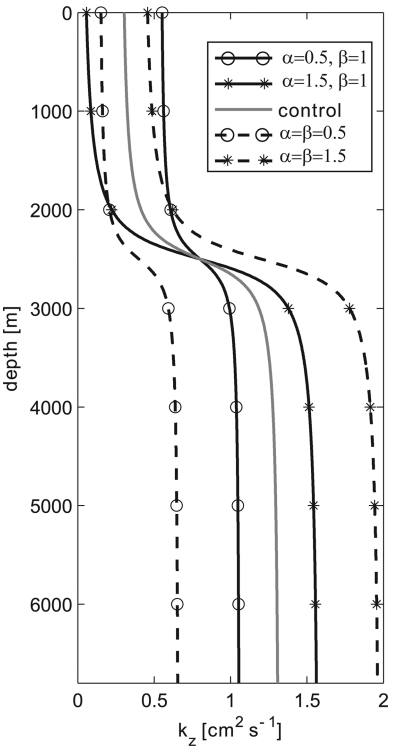

Figure 1. The vertical diffusivity used in the different cases in the model runs. The control run diffusivity is marked with a solid gray line, whereas solid black lines mark case 1 and dashed lines mark case 2 diffusivities. Circles mark $\alpha = 0.5$, and stars denote the structure for $\alpha = 1.5$ for both cases.

exchange of heat and freshwater between the atmosphere and ocean (Bigg and Wadley, 2001). The wind field is a fixed seasonal cycle, taken from the near-surface wind fields of the LGM atmospheric simulation of Dong and Valdes (1998). The sensitivity of the model to wind stress fields from other LGM atmospheric simulations has been tested and found not to be a significant factor in producing variability.

b. Simulations

The model was spun up from a state of rest with a uniform stratification and run for 6000 years for the unmodified LGM ocean (i.e., without any freshwater flux and an unmodified diffusivity), with relaxation toward climatology during the first 200 years. The orbital parameters used in the model are set to those appropriate for the LGM, and the atmospheric CO_2 concentration was 181 ppm (Raynaud *et al.*, 1993; Petit *et al.*, 1999). This run formed the starting point for all the subsequent runs. The modified diffusivity and/or freshwater

supply described below were implemented in model year 5500 and 6000, respectively. The simulations continued for another 1000 years to achieve a new steady state, and these 1000 years are discussed in the following. The runs are denoted "α–runs" when the mixing is altered (regardless of whether α or β is modified, see below) and "flood runs" when the extra freshwater flux is added. The flood runs included addition of a meltwater pulse at the ice-edge of the Laurentide Ice Sheet entering into Hudson Strait (e.g. Dowdeswell *et al.*, 1995; Levine and Bigg, 2008). The magnitude of the pulse (Qf) was taken to be 0.3 Sv based on upper estimates of the ice volume of the Laurentide Ice Sheet assuming a melting period of 500 years (Bischof, 2000). Changes in ocean mixing due to altered tidal dissipation rates were simulated in two ways to give a sensitivity range in the α-runs. Both involved modifying k_z by a setting α and/or β to 0.5, 1 or 1.5 ($\alpha = \beta = 1$ is thus a mixing control). In the first set of experiments (henceforth known as case 1), $\alpha = 0.5$ or 1.5 and $\beta = 1$, thus effectively changing the vertical gradient of the diffusivity. During the second set of simulations (case 2) $\alpha = \beta = 0.5$ or 1.5, thus changing the overall magnitude of the diffusivity.

The model output consisted of monthly averages of integrated volume transports in the large gyre systems, the overturning circulations and four major straits, and of total ice volumes in the Southern and Northern Hemisphere oceans and on land. In addition to the transports, snapshots of current velocities, stratification and variables from the atmospheric model were obtained every 100 model years, although focus here is on the state in January of year 6300 and 7000; i.e., after 300 years of flood (or 800 years of mixing) perturbation, and at the end of the simulation.

3. Results

a. Transports

The transports were originally output as monthly averages, but for ease of interpretation the data have been smoothed by application of a 12-month centered moving average. The model reached steady state by year 5500, which leads to an AMOC of 9.6 Sv and a Pacific MOC (PMOC) of 9.5 Sv (Fig. 2). In the flood case – where 0.3 Sv was added at Hudson Strait for 500 years starting at year 6000 – there is a near-collapse of the AMOC during the period of the pulse, but an increased PMOC, and a slight destabilization of the Southern Hemisphere overturning circulation (OC). This is associated with a weak decrease of the surface density in the North Atlantic (Fig. 3) from year 6300. Note that the ocean returns to a pre-pulse state within a century of the end of the pulse (Fig. 2), except in the Pacific, where a new, stronger, overturning state has been entered (cf., the MIS 6 results in Green *et al.,* 2011).

From the simulation with an altered diffusivity gradient (case 1; Fig. 4), we find a decreased AMOC, even with an increased α, compared to the control run (see Fig. 2). There are only minor changes to the transports for the run with $\alpha = 1.5$, but the low α-run sets up a strong PMOC at the expense of the AMOC. (cf., the case 2 with flood below). The PMOC changes significantly with altered diffusivity, and exhibits an increased circulation

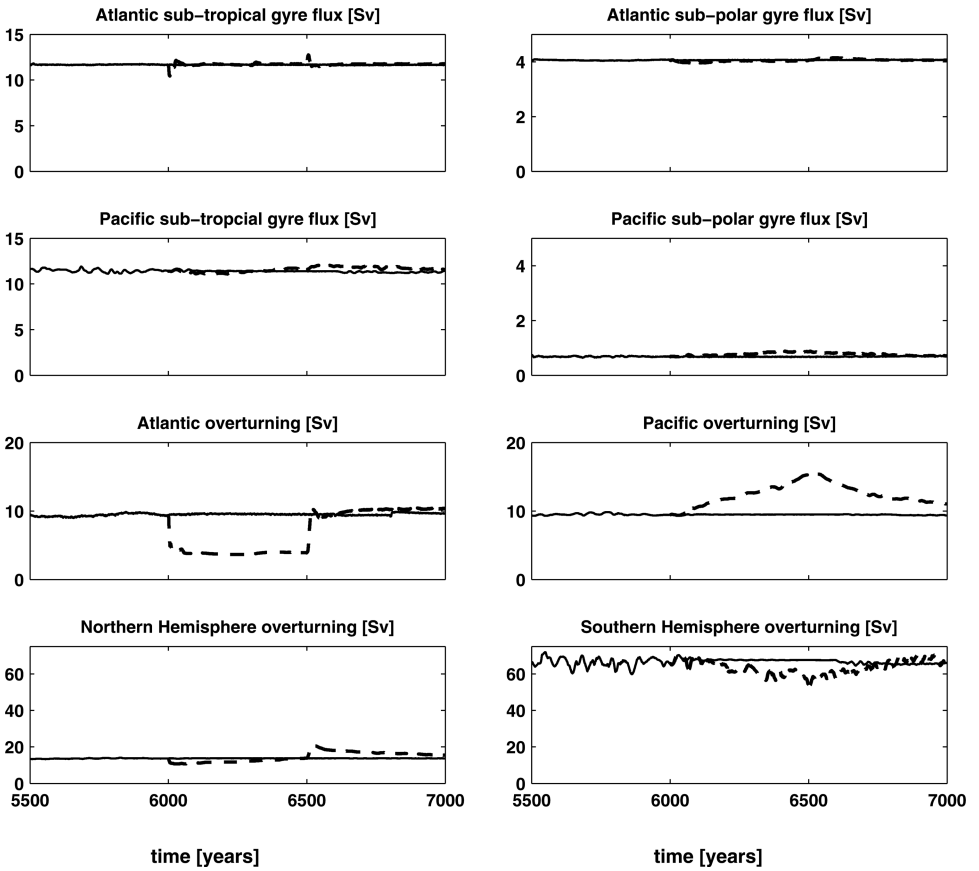

Figure 2. Transport time series for the control run (solid), and control run with Qf = 0.3 Sv added to the Hudson Bay (dotted/light). Note the different y-axis scales. All transports are in Sv [$= 10^6$ m^3 s^{-1}], and the data in this and further panels of transports have been smoothed using a 10-year moving average (see Bigg *et al.*, 2005 and Levine and Bigg, 2008 for comparisons and details).

with decreased α. In the flood runs for case 1, $\alpha = 0.5$, there is almost no effect on the AMOC, but the Southern Hemisphere OC changes significantly (Fig. 4). With $\alpha = 1.5$, there is a minor increase in the PMOC during the flood, whereas the $\alpha = 0.5$ run shows a similar picture to the no flood case, but with a slightly weaker circulation. These results are indeed surprising, and point toward the diffusivity in the *upper* ocean being a controlling factor in the simulations - case 1, $\alpha = 0.5$ has the highest diffusivity in the upper part of the water column whereas case 1, $\alpha = 1.5$ has the lowest (Fig. 1).

In the no flood run of case 2 (Fig. 5), there is only a small change in the $\alpha = 0.5$ case, but for $\alpha = 1.5$ the AMOC collapses and then (nearly) stabilizes. Again, we see a strong PMOC instead, which in combination with the relatively stable Southern Hemisphere overturning

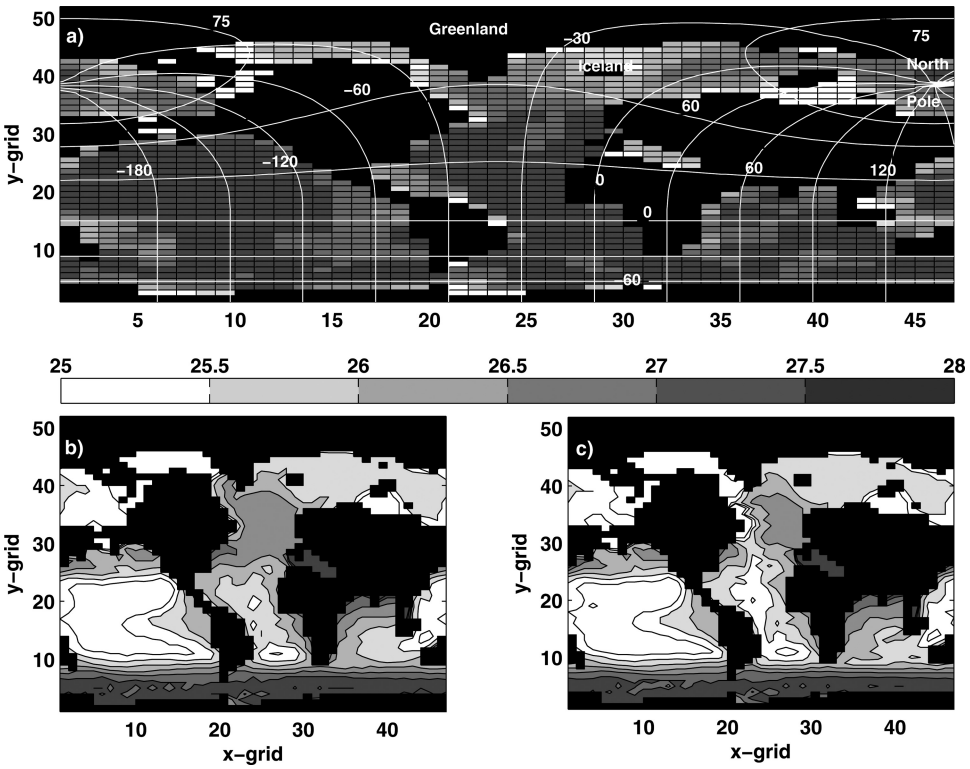

Figure 3. (a) The bathymetry (in grey) and gridcells shown on a Frugal projection, with latitude and longitude lines (in white) superposed. Labels for longitudes are placed within line, whereas those for latitudes are placed about or below the corresponding line. Note that the Frugal projection is used in all field plots in the following. (b) and (c) The surface density field, expressed as σ_0-1000, at year 6300 for the control (b) and control flood (b). Note that the colorbar refers to these two panels and not to the data shown in panel (a).

indicate a switch in the convection basin. The upper ocean diffusivity is higher than in the control for case 2 with $\alpha = 1.5$, and together with the results from case 1, $\alpha = 0.5$, this indicate that a high upper ocean diffusivity favors a dominating Pacific MOC. The subpolar North Atlantic gyre is far stronger in the large mixing case (whereas the subtropical gyre is weaker), indicating a more energetic North Atlantic and a weakened circulation farther south in the basin. The Pacific overturning behaves like previous reports have suggested for the AMOC: i.e., increasing with increased mixing (in the lower part of the water column). The case 2 runs with flooding show a weakened AMOC for both α-runs. However, with $\alpha = 1.5$ there is no trace of a recovery of the AMOC, whereas there is a slight improvement for $\alpha = 0.5$ (Fig. 5). There is no change in the PMOC for $\alpha = 0.5$, but a major increase for $\alpha = 1.5$ and significant changes in the subpolar and subtropical gyres.

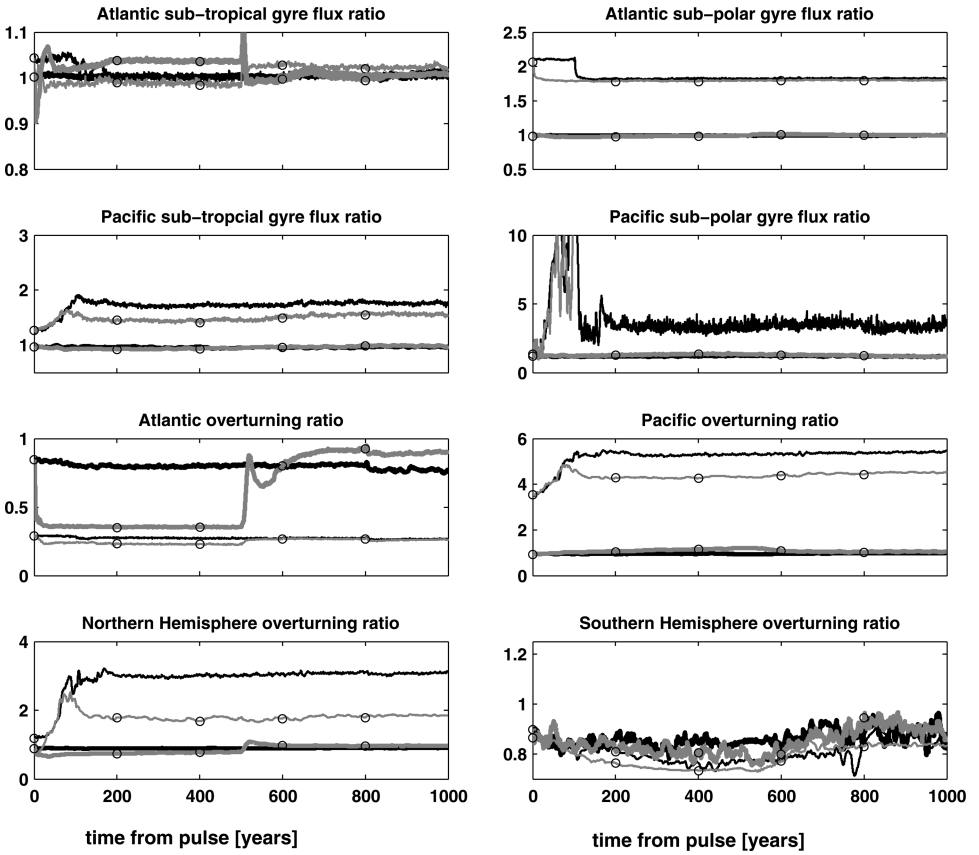

Figure 4. Transport ratios (perturbation over control) for case 1. No flood simulations are marked in black and flood runs in grey with black circles (note that the flood lasted 500 years starting at year 0 in this figure, equivalent to model year 6000). Thin lines represent $\alpha = 0.5$, heavy lines mark simulations with $\alpha = 1.5$. Note that for several of the panels lines lie on top of each other and may not be individually distinguished.

b. Stratification

The sea-surface temperature (SST) and salinity (SSS) at year 6300 for the control and control flood run are shown in Figure 6. The only major impact of the flood is on the (North) Atlantic SSS, although there is a small signal present in the Pacific SSS. The impact on SST is virtually negligible in the flood case. From the control cases and the transport results it appears that the impact of manipulating k_z surpasses effects of freshwater fluxes from the Laurentide Ice Sheet. In the following, focus is thus on the no-flood runs in order to determine the impact of the mixing.

The case 1 runs exhibit a large SSS maxima in the Pacific for $\alpha = 0.5$ (Fig. 7, top left panel) and a change in SST as well (warmer Pacific). The Arctic SSS minimum extends all

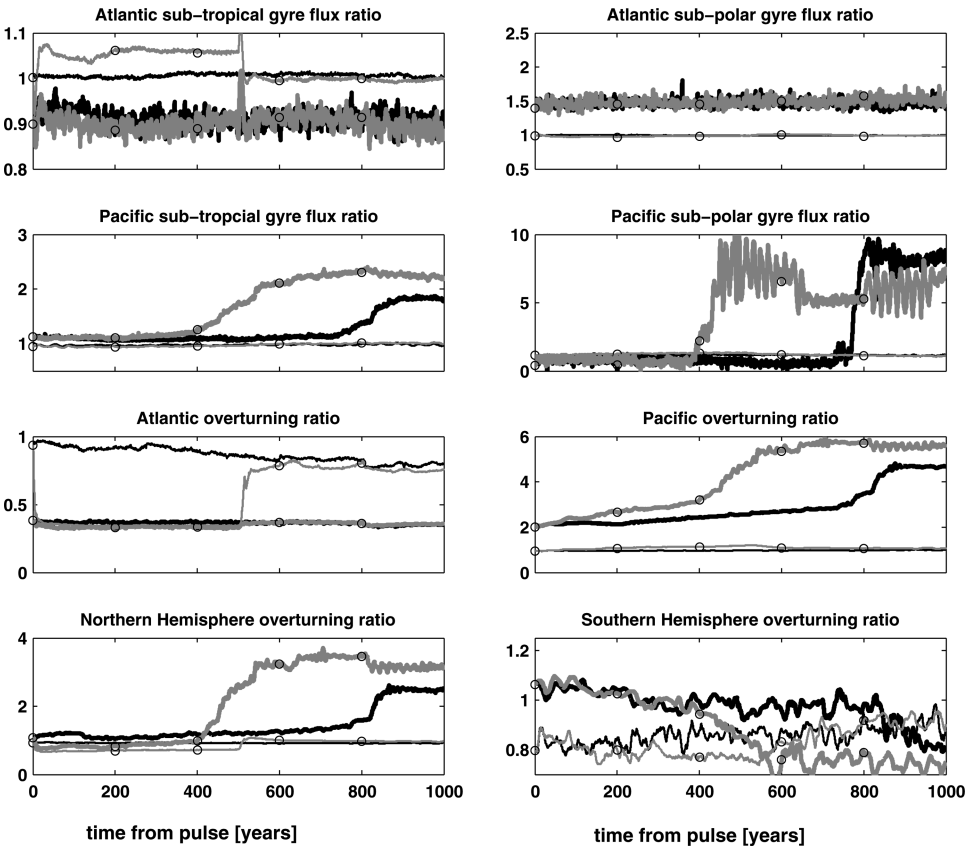

Figure 5. Transport ratios (perturbation over control) for case 2 simulations. No flood runs are marked in black and flood runs in grey with black circles. Thin lines represent $\alpha = 0.5$, heavy lines mark simulations with $\alpha = 1.5$. Note the different y-axis scales between panels and the previous figure, and that, again, lines lie on top of each other and may not be individually distinguished.

the way to the equator in the $\alpha = 0.5$ simulation. In fact, the entire surface layer seems to have freshened in this run, apart from in the Pacific. The $\alpha = 1.5$ run for case 1 shows a picture which resembles the control run (Fig. 6) more. This again supports the idea that the convective basin is set by the upper ocean diffusivity. This statement is strengthened by the case 2 results (Fig. 8), where there is a significant difference in the SSS with a saltier Pacific and fresher Atlantic in the $\alpha = 1.5$ simulations (second row), but only minor differences for $\alpha = 0.5$. There are no major changes in the SST for either of the α-runs for case 2.

Sea surface density fields are shown in Figure 9; we also show transects through the Atlantic (Fig. 10) and Pacific (Fig. 11) oceans. The deep-water convection takes place in the Atlantic in the control and for case 1, $\alpha = 1.5$ and case 2, $\alpha = 0.5$ (i.e., in the

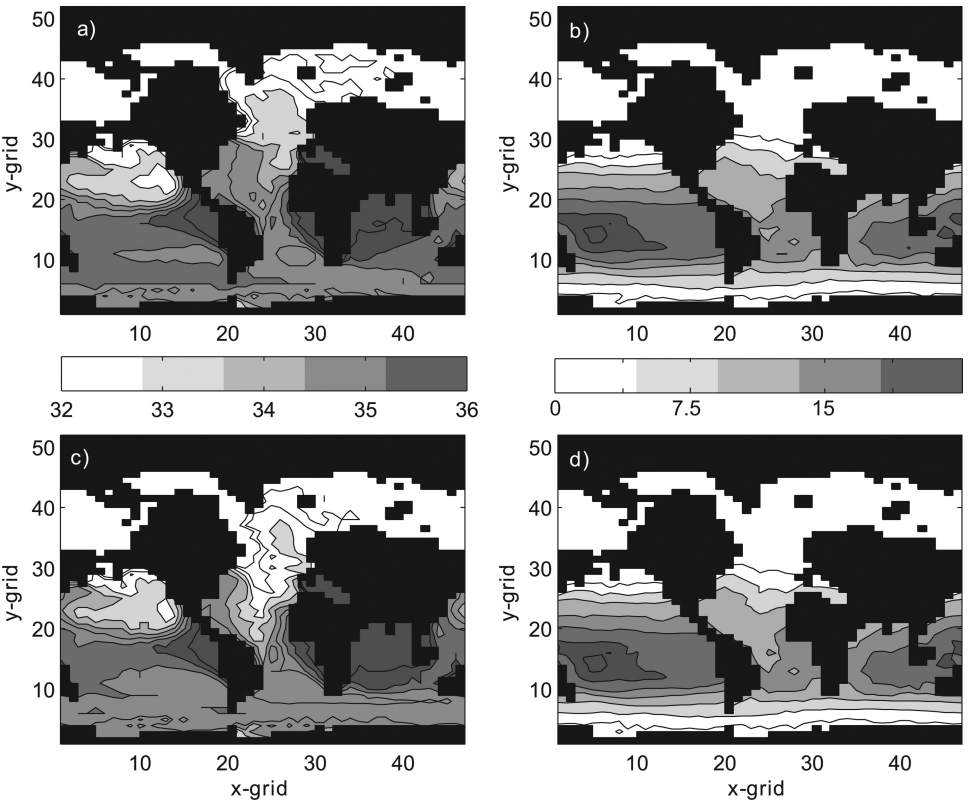

Figure 6. Modeled SSS (a and c, the unit is psu) and SST (b and d, in °C) at Year 6300 for the control (a-b) and flood run (c-d).

runs with lowest surface diffusivity). This again supports the hypothesis that low surface diffusivity leads to the Atlantic dominating, whereas stronger surface mixing sets up a Pacific domination. The transect figures further show that the abyssal ocean is filled with Southern Ocean water and that there is almost no density change between cases, and α-runs, beneath 3000–4000 m. Interestingly, in case 1, $\alpha = 0.5$ the convection in the Pacific reaches beneath 4000 m, whereas it does not penetrate beneath 2000 m in either basin in the other cases (this is supported by vertical velocity sections, which are not shown).

At the end of the simulations, i.e., model year 7000 (not shown), case 1 $\alpha = 0.5$ and case 2 $\alpha = 1.5$ show changes to the 6300-year state. In these simulations there is a complete removal of the Atlantic density maximum (case 1, $\alpha = 0.5$) and a weakened Pacific maximum (case 2, $\alpha = 1.5$), with associated changes in the vertical velocities. The switch to a Pacific convection is thus a long-term consequence of the altered mixing regime in the model.

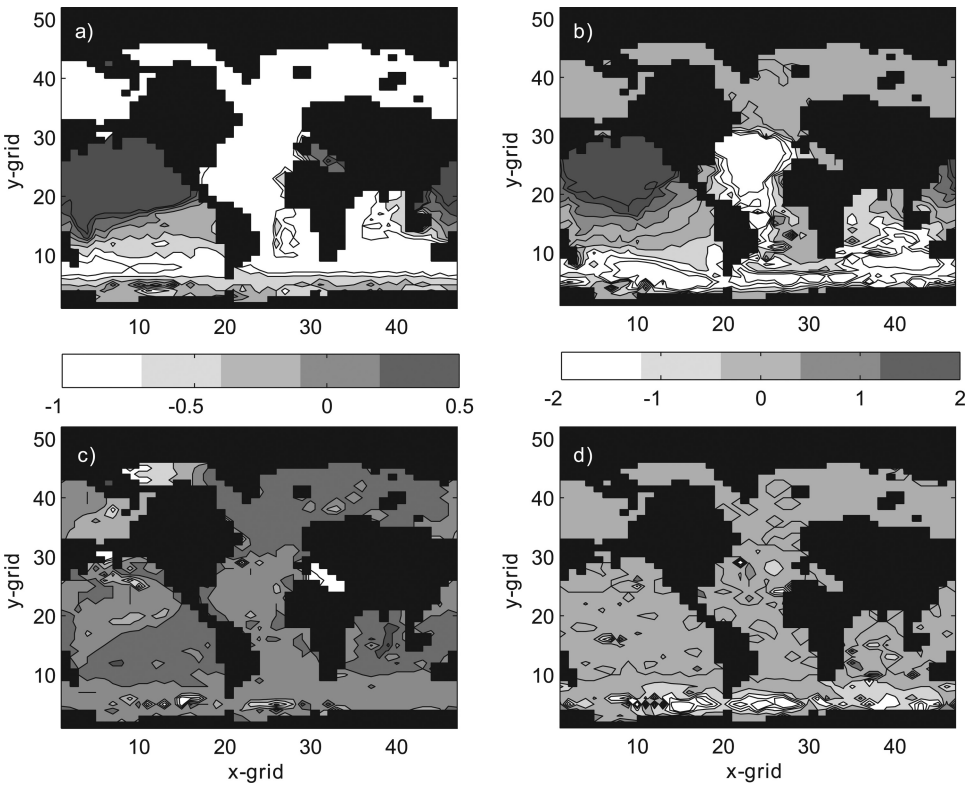

Figure 7. The differences between modeled SSS (a and c, the unit is psu) and SST (b and d, in °C) at Year 6300 for the case 1 runs without flooding and the control runs (Fig. 6). The top row shows results from $\alpha = 0.5$ whereas the second row shows $\alpha = 1.5$ results.

c. Freshwater content and dissipation

The response of the ocean is further quantified and described by calculation of the freshwater height, H_f defined by (e.g., Green *et al.*, 2004).

$$H_f = \int_{z_{ref}}^{0} \frac{S - S_{ref}}{S_{ref}} dz \tag{2}$$

Here $S_{ref} = 2200\,\text{m}$ is a reference depth taken far below the freshwater influenced surface layer, S is the salinity at a location, and z_{ref} is the salinity at the reference level at that location. Note that H_f is independent of the mixing as long as the contribution of the vertical flux past z_{ref} to the salinity above z_{ref} is small.

When Eq. (2) is applied to the control data, the expected results are found: the Atlantic and Arctic are fresher with the flood, but there is also a saltier North Pacific with the

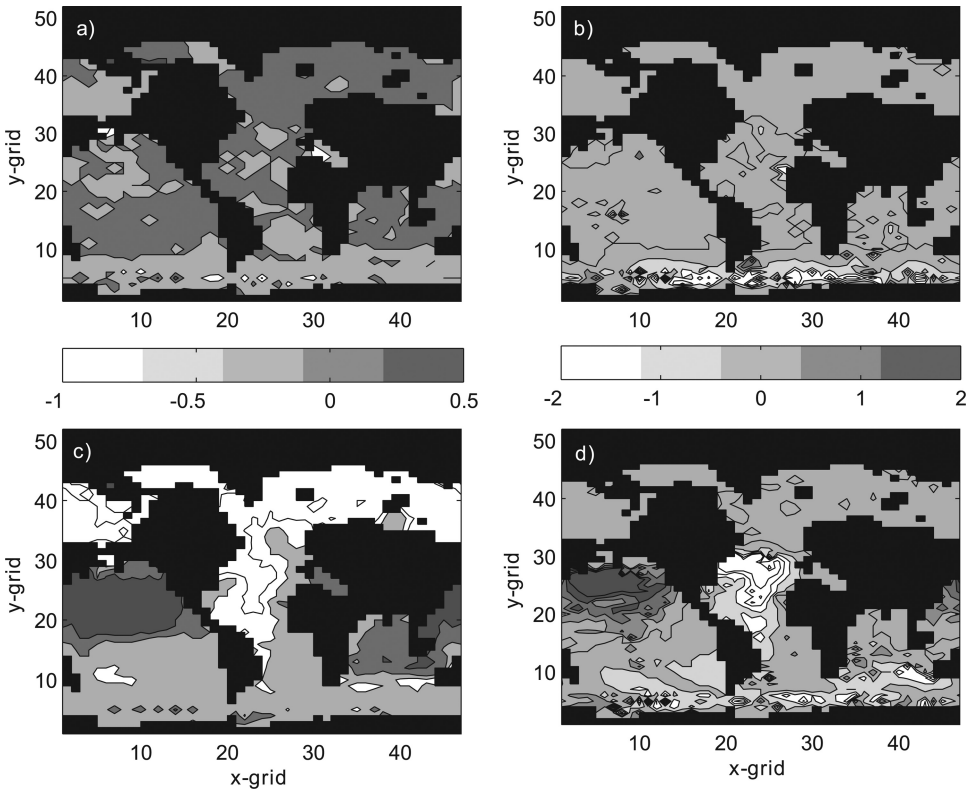

Figure 8. Shown is the difference between the SSS (panels a and c, the unit is psu) and SST (b and d, in °C) at Year 6300 for the case 2 runs without flooding and the control run (Fig. 6). The top row shows results from $\alpha = 0.5$ whereas the second row shows $\alpha = 1.5$ results.

extra freshwater (Fig. 12). By averaging the computed freshwater height over (somewhat arbitrarily chosen) areas of each basin, we produce Figure 13 (data are averaged over 10×10 grid cells; i.e., the surface area varies between each region but captures significant structures). For case 1, the freshwater height is proportional to α in the Pacific (panel a), which is opposite to the other cases and locations. In fact, the Pacific freshwater pool swaps place, from the south with $\alpha = 0.5$ to the north with $\alpha = 1.5$. Consequently, the freshwater maximum in the North Pacific is there in the 1.5 but not the 0.5 α-simulation. With $\alpha = 0.5$, the Atlantic (b) and Southern Oceans (c) are far fresher than in the control or $\alpha = 1.5$ runs, which explains the lack of freshwater in the (north) Pacific – it is distributed over other ocean basins instead, including the (western) Indian Ocean (panel d). Case 1 flood ($\alpha = 1.5$, marked with $*$) is pretty much identical to case 1 no flood (pentagram; again $\alpha = 1.5$). Note that case 1, $\alpha = 1.5$ has the lowest surface diffusivity but the second highest abyssal values of k_z. Case 1, $\alpha = 0.5$ is reversed, in that it has the highest surface k_z and the

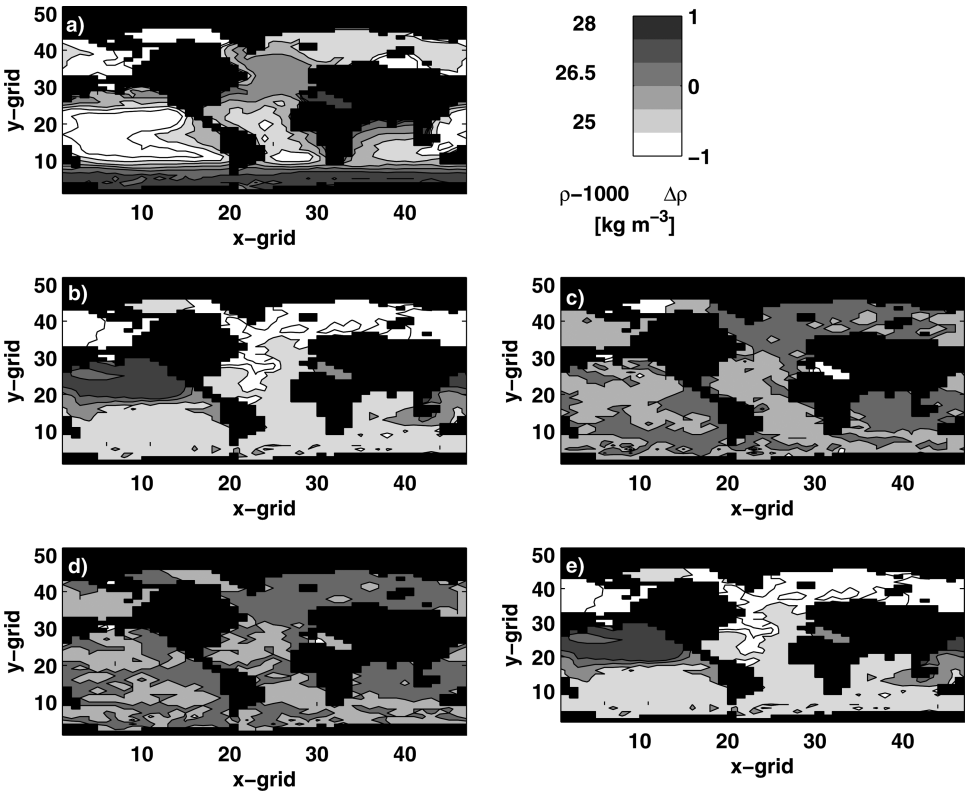

Figure 9. SS density at Year 6300 for control (panel a), and the difference between case 1 (panels b and c) and case 2 (d- e) and the control (i.e., panel a). All runs are without flooding, and for cases 1 and 2 left hand panels are for $\alpha = 0.5$ and right hand for $\alpha = 1.5$, respectively. Note the double colorbar, where the left-hand scale refers to panel a (showing the density), and the right hand scale refers to panels b-e (i.e., showing the difference).

second to lowest abyssal diffusivity. Case 2 no flood shows virtually no difference between $\alpha = 0.5$ and the control runs, but a quite strong signal in the Northern Hemisphere between control and $\alpha = 1.5$. There is a reversed structure in the Pacific for case 2 (not shown in detail) compared to the case 1 runs, with similar responses found for the case 2 flood, but with a larger freshwater height. These results imply that the presence of the North Pacific salinity minimum is determined by the diffusivity in the upper part of the water column, and it is present when k_z in the upper ocean is at a minimum.

There is a direct relationship between vertical diffusivity and the dissipation of turbulent kinetic (mechanical) energy (e.g., Osborn, 1980):

$$k_z = \Pi \frac{\varepsilon}{N^2} \tag{3}$$

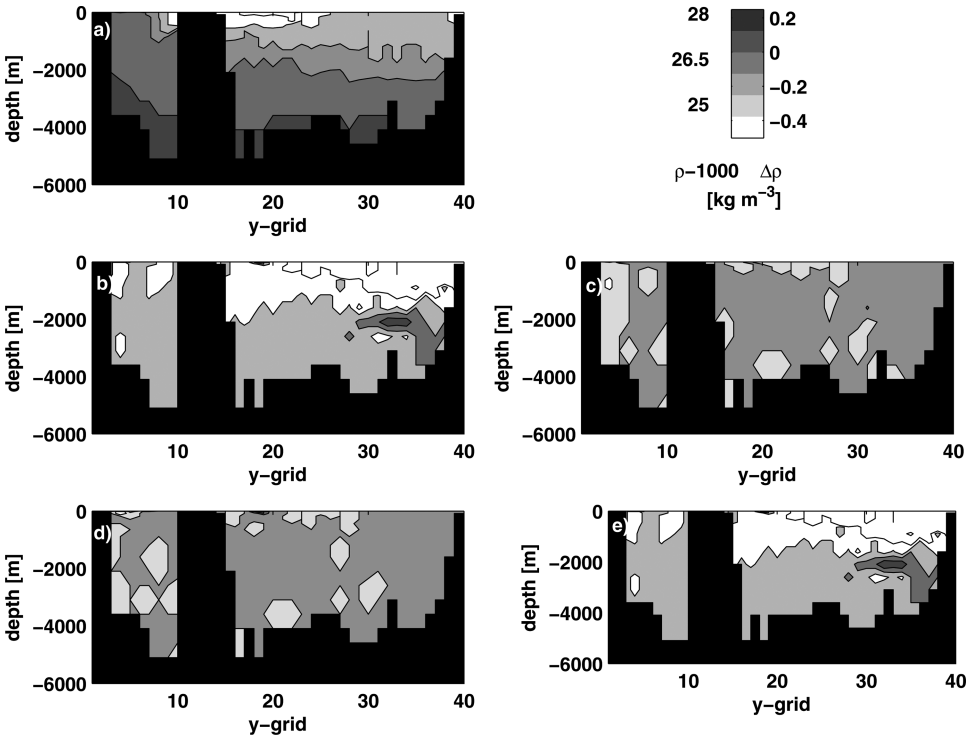

Figure 10. Density perturbation transects through the Atlantic Ocean (along x-grid cell 23; shown is again case-run minus control) at Year 6300 for control (top), case 1 (middle) and case 2 (lower). All runs are without flooding, and for cases 1-2, left-hand panels are for $\alpha = 0.5$ and right-hand panels for $\alpha = 1.5$, respectively. Note that the panels are cut above y-grid cell 40 as it only shows land (Greenland in the current projection), and that there is a double scale on the colorbar (see the caption for Fig. 9 for details).

where Π is a mixing efficiency (canonically taken to be equal to 0.2), ε is the dissipation rate, and $N^2 = -g/\sigma\partial\rho/\partial z$ is the buoyancy frequency (ρ is the density, and g acceleration due to gravity). By using the prescribed diffusivity in the model and the resulting modeled stratification to compute N^2 it is possible to estimate the implicit amount of energy dissipated in Frugal, to compare the different runs. The buoyancy frequency was computed for each grid cell and each vertical level using the output from years 6300 and 7000, and the associated dissipation rates were then estimated using Eq. (3). The resulting rates were then multiplied by the density, and averaged to produce the results in Table 1. It is obvious that the runs with a high upper ocean diffusivity experience, on average, stronger vertical stratification than the other runs. This in turn gives a high implicit dissipation rate in the model simulations. One can thus conclude that in the paleocean, where mixing rates were generally higher throughout the water column (e.g., Egbert *et al.*, 2004; Wunsch, 2005), case 2 with $\alpha = 1.5$ is a relevant approximation of the paleocean conditions.

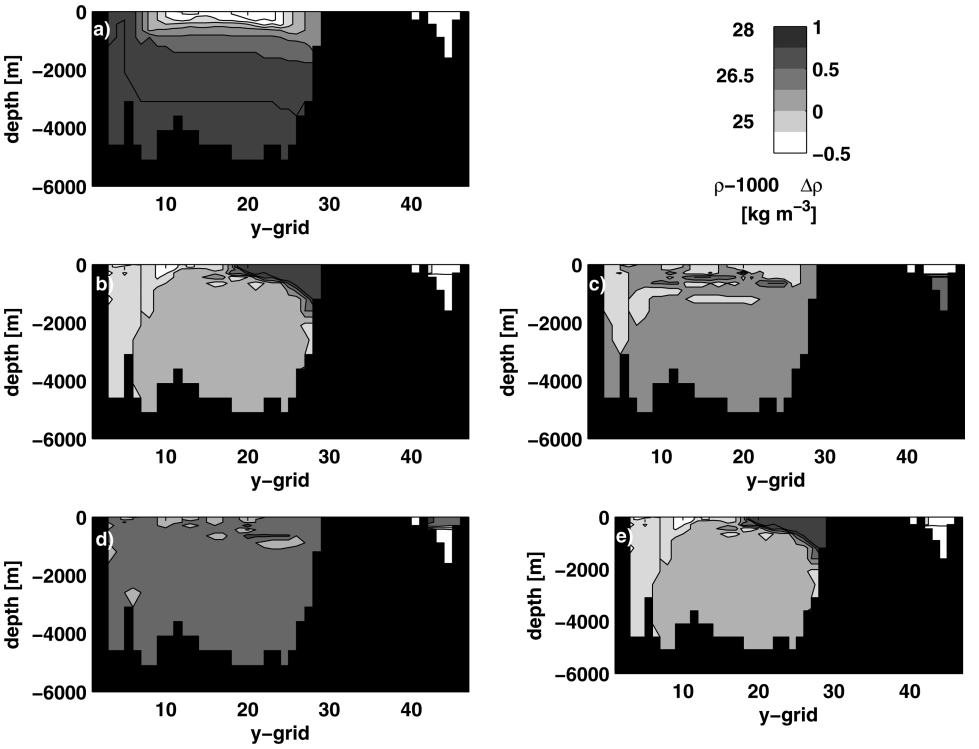

Figure 11. Density perturbation (case run minus control) transects through the Pacific Ocean (along x-grid cell 11) at Year 6300 for control (top), case 1 (middle) and case 2 (lower). All runs are without flooding, and for cases 1-2, left hand panels are for $\alpha = 0.5$ and right hand panels for $\alpha = 1.5$. Note that the panels are cut at y-grid cell 45 (i.e., the south coast of Greenland) to show changes in the Northwest Atlantic. Again, note the double colorbar scale (see Fig. 9).

d. A comparison to PD conditions

Running the model for Present Day (PD) conditions with case 2 mixing implemented produced the results shown in Figure 14 for the transports (see also Wadley *et al.*, 2002 and Green *et al.*, 2009). These simulations show a different picture to the paleo-results presented in this paper. Most notable is the directly proportional response of the Atlantic MOC to changed mixing, whereas the Pacific MOC is significantly weakened and the Pacific sub-polar gyre has practically collapsed. The Southern Hemisphere overturning increases by a factor of 4 in the $\alpha = 1.5$ run and 2.5 for $\alpha = 0.5$. There is thus a complex interaction between the strength of the vertical mixing, the overturning circulation, and other forcing parameters. For example, the paleocean experienced a signficantly stronger wind stress (not shown) over the North Pacific whereas the stress over the North Atlantic is more than halved compared to PD (but the stresses over land are almost an order of

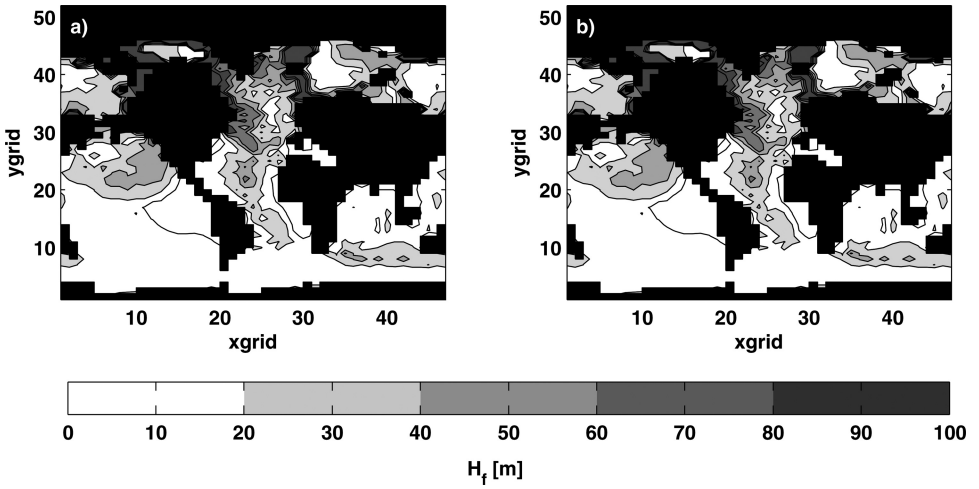

Figure 12. The freshwater height for the control (a) and control with flood (b) at model year 6300.

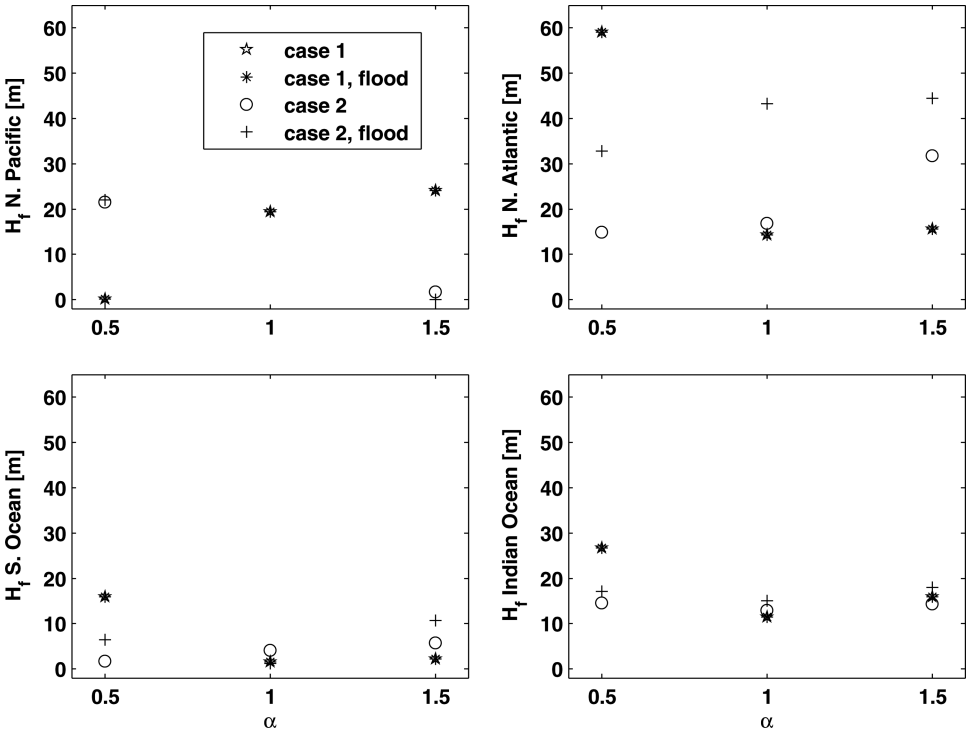

Figure 13. The average freshwater height at Year 6300 from the North Pacific (a), North Atlantic (b), the Southern Ocean (c), and the eastern Indian Ocean (d) as a function of α. See the text for more details.

Table 1. Global averaged buoyancy frequency from year 6300 and the associated implicit horizontally averaged dissipation rates from Eq. (3) for the different cases.

	N^2 $[\times 10^{-5}\,\mathrm{s}^{-1}]$	implicit ε $[\times 10^{-6}\,\mathrm{W\,m}^{-3}]$	comment
control	0.39	0.83	
control flood	0.41	0.87	
case 1, α = 0.5	**0.65**	2.03	**highest surface k_z**; second lowest bottom k_z
case 1, α = 1.5	0.41	0.42	lowest surface k_z; second highest bottom k_z
case 2, α = 0.5	0.40	0.42	second lowest surface k_z; lowest bottom k_z
case 2, α = 1.5	**0.45**	1.44	**second highest surface k_z**; highest bottom k_z
case 1, α = 0.5, flood	0.67	2.08	**highest surface k_z**; second lowest bottom k_z
case 1, α = 1.5, flood	0.43	0.45	lowest surface k_z; second highest bottom k_z
case 2, α = 0.5, flood	0.42	0.44	second lowest surface k_z; lowest bottom k_z
case 2, α = 1.5, flood	0.48	1.54	**second highest surface k_z**; highest bottom k_z

magnitude larger in the past – see a range of LGM and PD atmospheric model results at http://www.ncdc.noaa.gov/paleo/modelvis.html). This explains why the two periods experience such varied response to changes in mixing: if the atmospheric forcing changes, the response to ocean mixing changes as well because the wind-driven upper ocean circulation patterns are modified (note that there is a heat- and wind feedback between the atmospheric component and the ocean model in Frugal).

4. Discussion

The present simulations focus on the response of the ocean circulation to changed vertical mixing rates in combination with freshwater pulses from a collapsing Laurentide Ice Sheet. The conditions represent those at the end of the last glaciation, and with the pulse added at the Hudson Strait we roughly represent conditions from the Younger Dryas (albeit with a

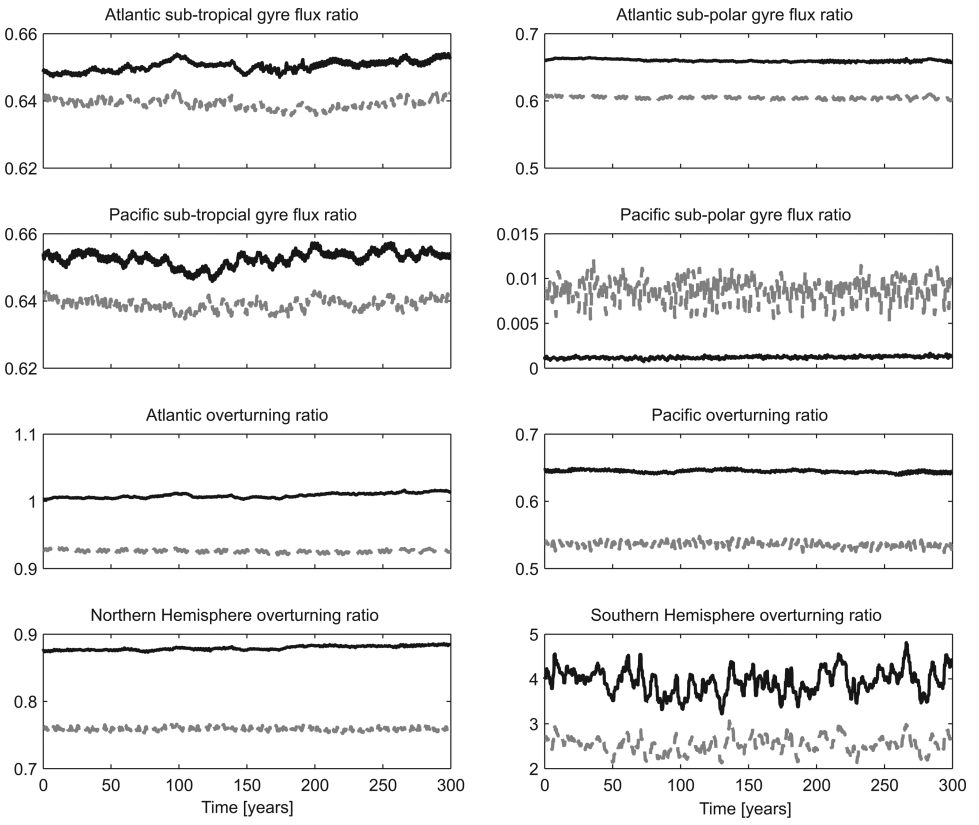

Figure 14. The ratio between the PD control run and the $\alpha = 0.5$ (dotted) and $\alpha = 1.5$ (thick solid) for a typical 300 year-long period starting at model year 6000.

lower sea-level; see also Levine and Bigg, 2008 and Bigg *et al.*, 2011). There is an inverse response between total (case 2) and gradient (case 1) mixing setups, and the upper ocean mixing rate determines which basin is the one with deep convection. When the upper ocean diffusivity is larger than in the control (i.e., case 1, $\alpha = 0.5$ and case 2, $\alpha = 1.5$) the Pacific is the dominating basin for deep water formation in the Northern Hemisphere. Reciprocally, when the upper ocean diffusivity is low, the Atlantic is the dominating basin for convection. Catastrophic releases of freshwater from surrounding ice sheets do not alter this, but merely dictate the strength of the AMOC. However, in runs with large upper ocean diffusivity the AMOC is more sensitive and does not recover to control conditions after the freshwater pulse has ended. This may be further enhanced by the fact that the horizontal surface area of the (north) Pacific is much larger than the Arctic and Atlantic, so a larger upper ocean vertical diffusivity can simply transfer more water vertically, which would mean a generally saltier upper ocean and possibly a fresher lower layer. The temperature is affected to a lesser

extent as the vertical temperature structure in the upper ocean is mainly determined by direct wind mixing and surface heat input, and these are only weakly linked to SSS-changes and thus the vertical diffusivity. The exact mechanism is far from clear, however, and it is possible that the weak response to decreased upper ocean diffusivity is simply because the diffusivity becomes so low that, although the Pacific is larger, the diffusivity has no effect or is superseded by other processes (e.g., the isopycnal diffusivity added in the mixing scheme or missing feedbacks from the closed Bering Strait). Furthermore, there is only a minor impact on the MOCs by the vertical diffusivity in the lower part of the water column. This may be because, in terms of salinity and temperature, the deeper ocean is "fed" only by deep water formation, mainly from the Southern Ocean in terms of volume fluxes, and the Southern Hemisphere overturning does not change significantly in the simulations (Fig. 2, 4-7). Thus we will see a more vertically well mixed deep ocean in our increased mixing runs, but it cannot impact the freshwater content and transports.

There are indications that the ocean at the termination of the last glacial may have been more sensitive to changes in forcing than during MIS 6 (Green *et al.*, 2011). The simulations here show the sensitivity of the circulation to changes in vertical mixing, and point toward intricate connections and feedbacks between the processes acting on the ocean circulation. Many proxy-based paleoceanographic studies demonstrate rapid recovery following periods of MOC breakdown or shut down, e.g. after Heinrich events or Dansgaard-Oeschger stadials (e.g., McManus *et al*., 2004). The increased supply of mechanical energy was not sufficient to counteract the changes in vertical stratification due to freshwater fluxes, but a stronger tidal mixing in the deeper regions of the LGM ocean, which would have kept the weaker upper ocean state in relation to the diffusivity at depth, may have helped to maintain the MOC in a fresher environment and contributed to its ability to recover after such catastrophic events. A reduction of the Atlantic MOC leads to a colder Arctic and North Atlantic, which in turn induces a larger equator-pole temperature gradient with potentially increased winds as a result. The current investigation is a sensitivity study more than an attempt to represent actual conditions during the LGM (to begin with, that would require a spatially varying diffusivity), but the above idea should lead to an increased upper-ocean mixing which in combination with a sustained larger deep-water mixing due to tidal resonance would mean that case 2, $\alpha = 1.5$ is the best representation (albeit possibly exaggerated in the surface but not in the deeper parts) of the mixing in the ocean during the Younger Dryas (e.g., Wunsch, 2005; Green, 2010). Kahana *et al.* (2004) report similar responses in their box model (except for the Pacific convection which they are physically unable to reproduce) with a mode with North Atlantic upwelling rather occurring when large freshwater pulses were added to the northern Atlantic, and bottom water production occurring in the Indian and Pacific oceans if the surface density was significantly altered. Thus, the present results have support in a variety of other sources. It is therefore possible that the balance of Atlantic to Pacific convection kept changing between the different glacial periods during the Quaternary due to a combination of altered oceanic mixing (through lowered sea level, modified tides and wind fields) and modified (vertical) stratifications.

Because of the horizontal resolution of the North Atlantic being finer than in the Southern and Pacific Oceans, the deep water formation ratio between the North Atlantic and Southern Ocean may be affected. It is thus likely that the North Atlantic MOC is overestimated and the Southern Ocean and Pacific MOC are underestimated. Nevertheless, this has not been a major issue in past FRUGAL simulations of the PD, LGM, and MIS 6 (see Bigg *et al.*, 2005; Levine and Bigg, 2008; and Green *et al.*, 2011 for details), and it has been extensively validated for the present (compared to observations) and the LGM and MIS 6 (compared to proxies) with regard to the large-scale pattern. Another potential issue with the present investigation is the relatively low vertical resolution. However, the large-scale ocean structure and circulation have scales spanning several vertical grid points, and we argue that the estimates are valid. The horizontally homogenous vertical background diffusivity is also a relatively crude approximation, and the MOC is sensitive to the structure as well as the magnitude of the mixing (Samelson, 1998; Huang, 1999; Schmittner *et al.*, 2003). However, with the present resolution, the horizontal structure of the vertical diffusivity in the ocean should be relatively weak and smeared out (e.g. Green, 2010) and thus have weak effects on the results. Work is planned to improve the diffusivity scheme in Frugal, especially in a higher-resolution version of the model. Vertical mixing is notoriously poorly represented in large-scale models (see Zickfeld *et al.*, 2007), and the present results again show the sensitivity of ocean models to varying mixing. It is concluded, just as in the previous investigation by Green *et al.* (2009) that it would be more appropriate to define the dissipation in ocean models, and let the diffusivity evolve with the stratification.

Acknowledgments. The manuscript was greatly improved by comments from two anonymous reviewers. JAMG acknowledges an Advanced Fellowship from the Natural Environmental Research Council through grant NE/F014821/1, as well as funding from C3W – the Climate Change Consortium of Wales.

REFERENCES

Alley, R. B. 1998. Icing the North Atlantic. Nature, *392*, 335–337.

Bigg, G. R., R. C. Levine and C.L. Green. 2011. Modelling abrupt glacial North Atlantic freshening: rates of change and their implications for Heinrich events. Glob. Plan. Change, (in press).

Bigg, G. R., S. R. Dye and M. R. Wadley. 2005. Interannual variability in the 1990s in the northern Atlantic and Nordic Seas. J. Atm. Ocean Sci., *10*, 123–143.

Bigg, G. R. and M. R. Wadley. 2001. Millennial-scale variability in the oceans: an ocean modelling view, J. Quat. Sci., *16*, 309–319.

Bigg, G. R., M. R. Wadley, D. P. Stevens and J. Johnson. 1998. Simulations of two last glacial maximum ocean states, Paleocean., *13*, 340–351.

—— 2000. Glacial thermohaline circulation states of the northern Atlantic: the compatibility of modelling and observations. J. Geol. Soc. London, *157*, 655–665.

Bischof, J. 2000. Ice Drift, Ocean Circulation and Climate Change, Springer Verlag, Berlin, 215 pp.

Bradley, R. S., ed. 1999. Paleoclimatology, 2nd ed., Academic Press, San Diego, 610 pp.

Broecker, W. S. and G. H. Denton. 1990. What drives glacial cycles? Sci. Am., *262*, 48–56.

Bryan, K. and L. J. Lewis. 1979. A water mass model of the world ocean. J. Geophys. Res., *84*, 2503–2517.

Dong, B. and P. J. Valdes. 1998. Simulations of the Last Glacial Maximum climates using a general circulation model: prescribed versus computed sea surface temperatures. Clim. Dyn., *14*, 571–591.

Dowdeswell, J. A., M. A. Maslin, J. T. Andrews and I. McCave. 1995. Iceberg production, debris rafting, and the extent of Heinrich layers, H-1, H-2 in North Atlantic sediments. Geology, *23*, 301–304.

Duplessy, J. 2004. Global ocean circulation and its past variations. Comptes Rendus Geoscience, *336*, 657–666.

Egbert, G. D., B. G. Bills and R. D. Ray. 2004. Numerical modeling of the global semidiurnal tide in the present day and in the last glacial maximum. J. Geophys. Res., *109*, C03003, doi:10.1029/2003JC001973.

England, M. H. 1993. Representing the global-scale water masses in ocean general circulation models. J. Phys. Oceanogr., *23*, 1523–1552.

Fairbanks, R. G. 1989. A 17, 000 year glacio-eustatic sea level record: influence of glacial melting rates on the Younger Dryas event and deep ocean circulation. Nature, *342*, 637–642.

Fanning, A. F. and A. J. Weaver. 1996. An atmospheric energy-moisture balance model: Climatology, interpentadal climate change, and coupling to an ocean general circulation model. J. Geophys. Res., *10*, 15111–15128.

Green, C. L., G. R. Bigg and J. A. M. Green. 2010. Deep draft icebergs from the Barents ice sheet during MIS 6 are consistent with erosional evidence from the Lomonosov ridge, central Arctic. Geophys. Res. Lett., *37*, L23606, doi:10.1029/2010GL045299.

Green, C. L., J. A. M. Green and G. R. Bigg. 2011. Simulating the impact of freshwater surges and deep-draft icebergs from the MIS 6 Barents Ice Sheet Collapse. Paleoceanogr., *26*, doi:10.1029/2010PA002088.

Green, J. A. M. 2010. Ocean tides and resonance. Ocean Dyn., *60*, 1243–1253, doi: 10.1007/s10236-010-0331-1.

Green, J. A. M., C. L. Green, G. R. Bigg, T. P. Rippeth, J. D. Scourse and K. Uehara. 2009. Tidal mixing and the meridional overturning circulation from the last glacial maximum. Geophys. Res. Lett., *36*, L15, 603, doi: 10.1029/2009GL039, 309.

Green, J. A. M., J. Molvaer and A. Stigebrandt. 2004, Hydrographic response of Holandsfjord to changed freshwater runoff, J. Geophys. Res., *109*, C07021.

Griffies, S. M., A. Gnanadesikan, R. C. Pacanowski, V. Larichev, J. K. Dukowicz and R. D. Smith. 1998. Isoneutral diffusion in a z-coordinate ocean model. J. Phys. Oceanogr., *28*, 831–841.

Huang, R. X. 1999. Mixing and energetics of the oceanic thermohaline circulation. J. Phys. Oceanogr., *29*, 727–746.

Kahana, R., G. R. Bigg and M. R. Wadley. 2004. Global ocean circulation modes derived from a multiple box model. J. Phys. Oceanogr., *34*, 1811–1823.

Keigwin, L. D., G. A. Jones, S. J. Lehman and E. A. Boyle. 1991. Deglacial meltwater discharge, North Atlantic deep circulation, and abrupt climate change. J. Geophys. Res., *96*, 16811–16826.

Lenderink, G. and R.J. Haarsma. 1994. Variability and multiple equilibria of the thermohaline circulation, associated with deep water formation. J. Phys. Oceanogr., *24*, 1480–1493.

Levine, R. C. and G. R. Bigg. 2008. The sensitivity of the glacial ocean to Heinrich events from different sources, as modeled by a coupled atmosphere-iceberg-ocean model. Paleoceanogr., *23*, PA4213, doi:10.1029/2008PA001, 613.

MacAyeal, D. R. 1993. Binge/purge oscillations of the Laurentide Ice-sheet as a cause of the North-Atlantics Heinrich events. Paleoceanogr., *8*, 775–784.

Marzeion, B., and A. Levermann. 2009. Stratification-dependent mixing may increase sensitivity of a wind-driven Atlantic overturning to surface freshwater flux. Geophys. Res. Lett., *36*, L20602, doi:10.1029/2009GL039947.

McManus, J., R. Francois, J. Gherardi, L. Keigwin and S. Brown-Leger. 2004. Collapse and rapid resumption of Atlantic meridional circulation linked to deglacial climate changes. Nature, *428*, 834–837.

Murton, J. B., M. D. Bateman, S. R. Dallimore, J. T. Teller and Z. Yang, Z. 2010. Mackenzie outburst flooding into the Arctic Ocean at the start of the Younger Dryas. Nature, *464*, 740–743.

Okumura, Y. M., C. Deser, A. X. Hu, A. Timmermann and S.-P. Xie. 2009. North Pacific climate response to freshwater forcing in the subarctic north Atlantic: Oceanic and atmospheric pathways. J. Climate, *22*, 1424–1445.

Osborn, T. R. 1980. Estimates of the local rate of vertical diffusion for dissipation measurements. J. Phys. Oceanogr., *10*, 83–89.

Peltier, W. 2004. Global glacial isostasy and the surface of the ice-age Earth: The ICE-5G (VM2) model and grace. Annu. Rev. Earth Planet.Sci., *32*, 111–149.

Petit, J. R. *et al.* 1999, Climate and atmospheric history of the past 420,000 years from the Vostok ice core, Antarctica. Nature, *399*, 429–436.

Rahmstorf, S. 2002 Ocean circulation and climate during the past 120,000 years. Nature, *419*, 207–214.

Raynaud, D., J. Jouzel, J. M. Barnola, J. Chapellaz, R. J. Delmas and C. Lorius. 1993. The ice record of greenhouse gases. Science, *259*, 926–934.

Samelson, R. M. 1998. Large-scale circulation with locally enhanced vertical mixing. J. Phys. Oceanogr., *28*, 721–726.

Schmittner, A., O. A. Saenko. and A. J. Weaver. 2003. Coupling of the hemisphere in observations and simulations of glacial climate change. Quat. Sci. Rev., *22*, 659–671.

Seidov, D. and M. Maslin. 1999. North Atlantic deep water circulation collapse during Heinrich events. Geology, *27*, 23–26.

Stouffer, R. J., K. W. Dixon, M. J. Spelman, W. J. Hurlin, J. Yin, J. M. Gregory, A. J. Weaver, M. Eby, G. M. Flato, D. Y. Robitaille, H. Hasumi, A. Oka, A. Hu, J. H. Jungclaus, I. V. Kamenkovich, A. Levermann, M. Montoya, S. Murakami, S. Nawrath, W. R. Peltier, G. Vettoretti, A. P. Sokolov and S. L. Weber. 2006. Investigating the causes of the response of the thermohaline circulation to past and future climate changes. J. Climate, *19*, doi:10.1175/JCLI3689.11.

Swingedouw, D., J. Mignot, P. Braconnot, E. Mosquet, M. Kageyama and R. Alkama. 2009. Impact of freshwater release in the North Atlantic under different climate conditions in an OAGCM. J. Climate, *22*, 6377–6403.

Teller, J. T., M. Boyd, Z. R. Yang, P. S. G. Kor and A. M. Fard. 2005.Alternative routing of Lake Agassiz overflow during the Younger Dryas: new dates, paleotopography, and a re-evaluation. Quat. Sci. Rev., *24*, 1890–1905.

Vellinga, M. and R. Wood. 2002. Global climatic impacts of a collapse of the Atlantic thermohaline circulation. Climatic Change, *54*, 251–268.

Wadley, M. R. and G. R. Bigg. 1999. Implementation of variable time stepping in an ocean general circulation model. Ocean Model., *1*, 71–80.

—— 2002. Impact of flow through the Canadian archipelago and Bering Strait on the North Atlantic and Arctic circulation: An ocean modelling study. Quart. J. Royal Met. Soc., *128*, 2187–2203.

Wadley, M. R., G. R. Bigg, E. J. Rohling and A. J. Payne. 2002, On modelling present day and last glacial maximum oceanic δ^{18}O distribution. Global Planet Change, *32*, 89–109.

Wunsch, C. 2005. Speculations on a schematic theory of the Younger Dryas. J. Mar. Res., *63*, 315–333.

Wunsch, C. and R. Ferrari. 2004. Vertical mixing, energy, and the general circulation of the oceans. Ann. Rev. Fluid Mech., *36*, 281–314.

Yokoyama, Y., K. Lambeck, P. D. Deckker, P. Johnston and L. K. Fifield. 2000. Timing of the last glacial maximum from observed sea-level minima. Nature, *406*, 713–716.

Zhang, R. and T. L. Delworth. 2005. Simulated tropical response to a substantial weakening of the Atlantic thermohaline circulation. J. Climate, *18*, doi:10.1175/JCLI34601.

Zickfeld, K., A. Levermann, M. G. Morgan, T. Kuhlbrodt, S. Rahmstorf and D. W. Keith. 2007. Expert judgments on the response of the Atlantic meridional overturning circulation to climate change. Climatic Change, *83*, 235–265.

Received: *11 January, 2011*; revised: *28 March, 2011*.